# Supplementary Information

## A Self-Buffering Structure for Application in High-Performance Sodium-Ion Batteries

*Zhiming Liu[a], Chuang Yue[a], Chaoji Chen[b], Juan Xiang[a], Fang Hu[a], Dongsoo Lee[a], Donghyeok Shin[a], Seho Sun[a], Liangbing Hu[b]*, Taeseup Song[a]**

[a] Department of Energy Engineering, Hanyang University, 222 Wangsimni-ro, Seongdong-gu, Seoul, 04763, Korea.

[b] Department of Materials Science and Engineering, University of Maryland, College Park, Maryland 20742, USA.

E-mail: binghu@umd.edu; tssong@hanyang.ac.kr

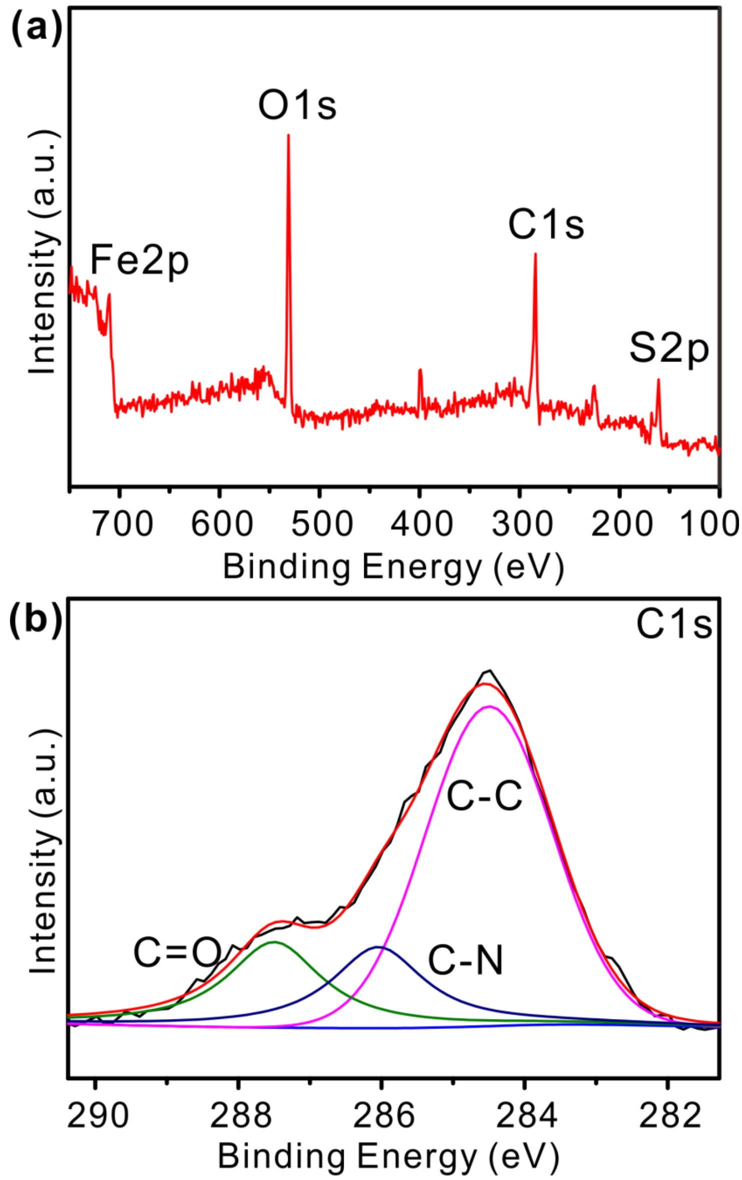


**Figure 1S.** (a) Survey XPS spectra of the S-$Fe_7S_8$ and (b) high-resolution C 1s XPS spectrum.

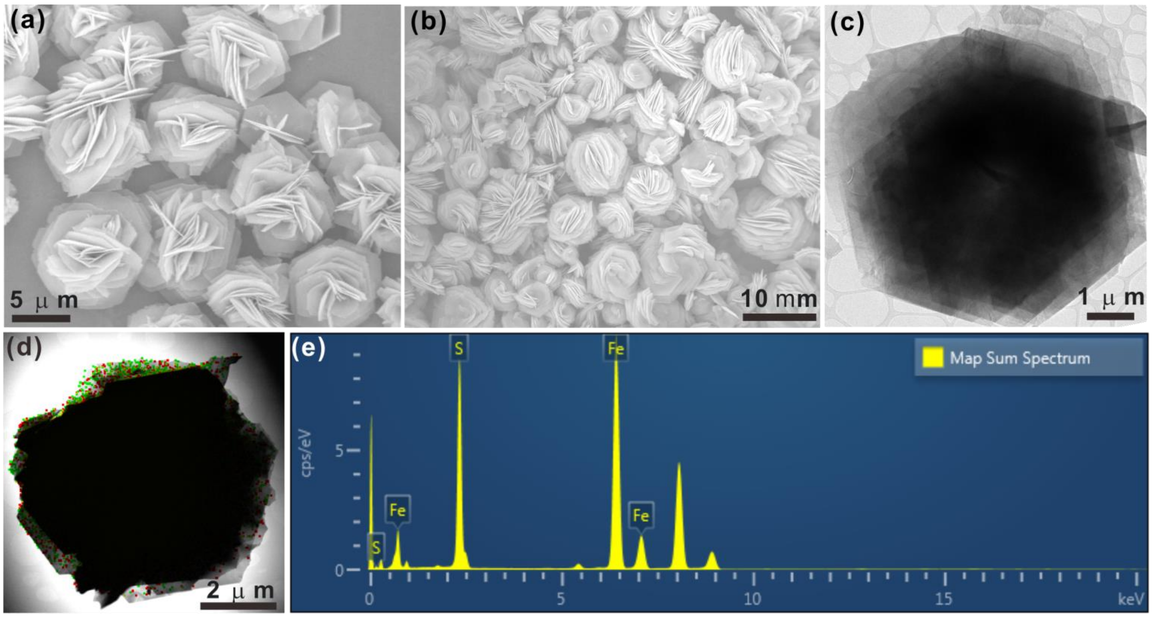


| (f) Element | Line Type | k Factor | k Factor type | Absorption Correction | Wt% | Wt% Sigma | Atomic % |
|---|---|---|---|---|---|---|---|
| S | K series | 1.047 | | 1.00 | 35.97 | 0.14 | 49.45 |
| Fe | K series | 1.047 | | 1.00 | 64.03 | 0.14 | 50.55 |
| Total: | | | | | 100.00 | | 100.00 |

**Figure S2.** Characterizations of S-$Fe_7S_8$: (a, b) SEM images, (c) TEM image, (d) dark-field TEM image, and (e, f) the corresponding information of a representative EDX spectrum.

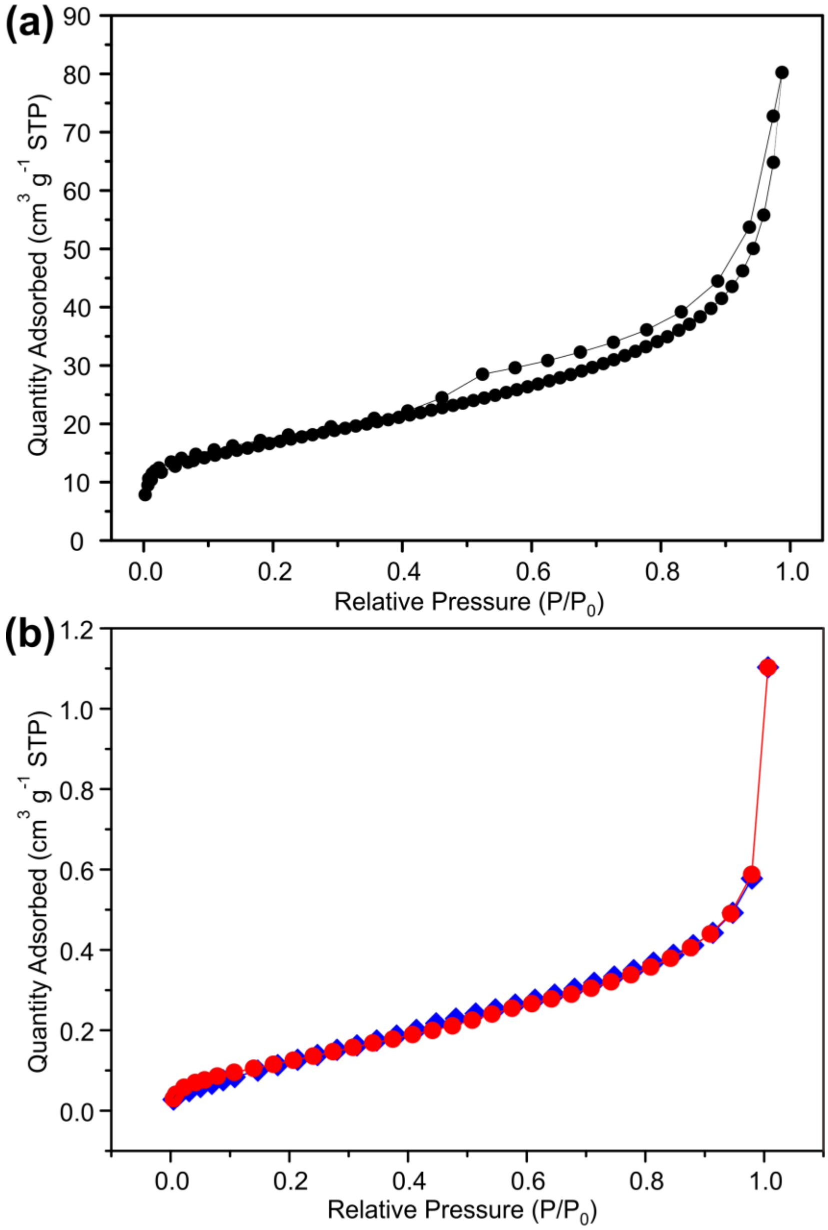


**Figure S3.** Nitrogen adsorption-desorption isotherm of (a) S-$Fe_7S_8$ and (b) B- $Fe_7S_8$.

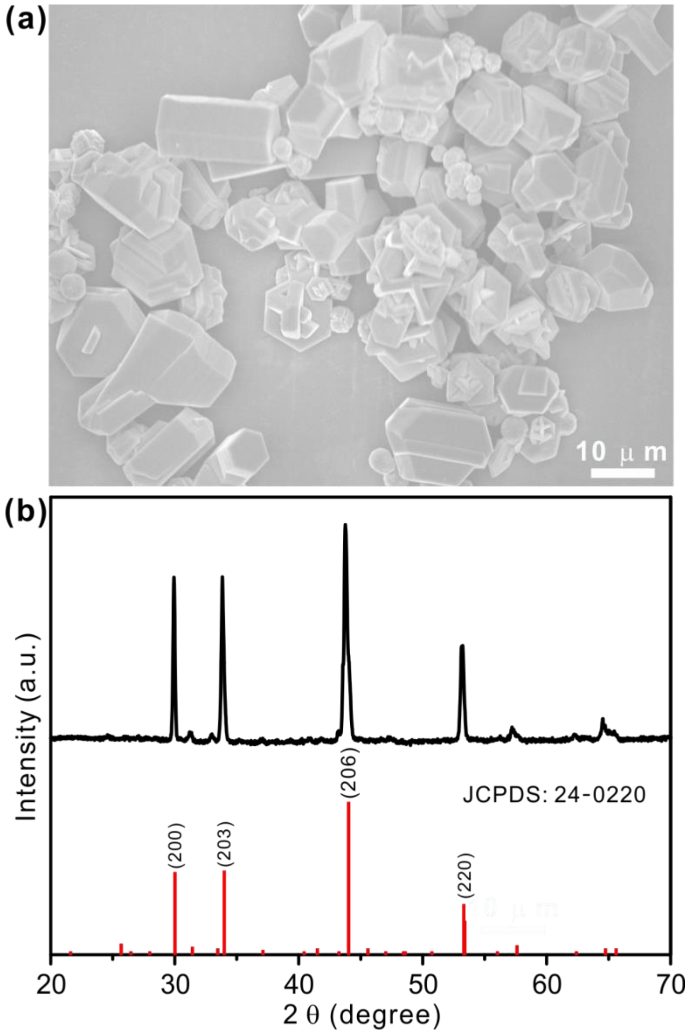


**Figure S4.** FESEM image and XRD parrtens of B-$Fe_7S_8$.

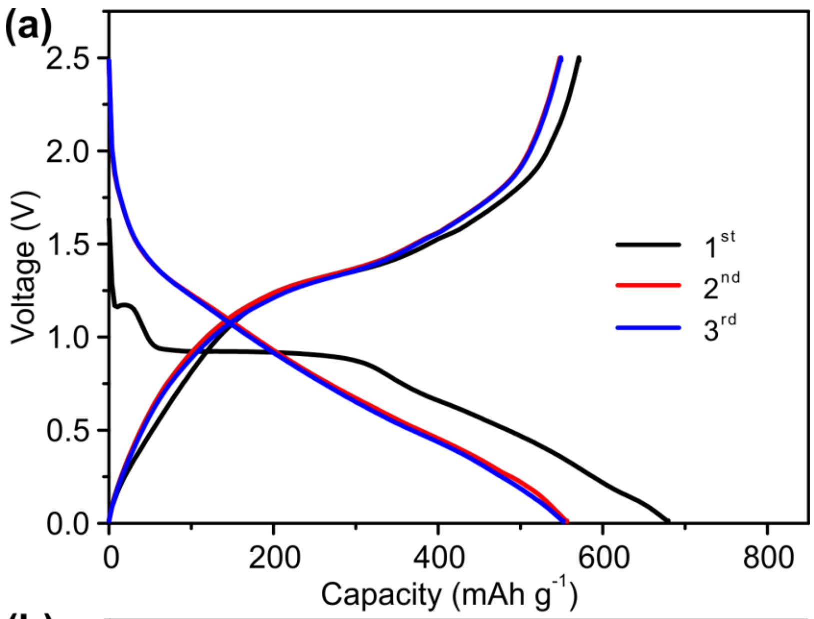


**Figure S5.** (a) Voltage profiles of S-$Fe_7S_8$ between 0.01 and 2.5 V at a current rate of 0.4C. (b) Voltage profiles of B-$Fe_7S_8$ between 0.2 and 2.5 V at a current rate of 0.4C.

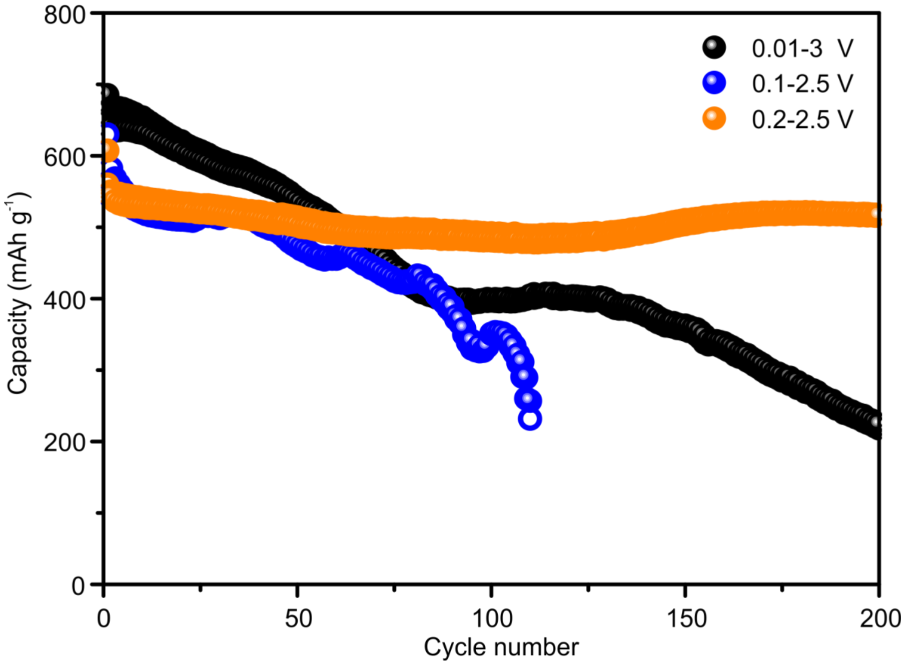


**Figure S6**. Cycling performance of S-$Fe_7S_8$ at a current rate of 1C with different cut-off voltage of 0.01-3 V, 0.1-2.5 V, and 0.2-2.5 V, respectively.

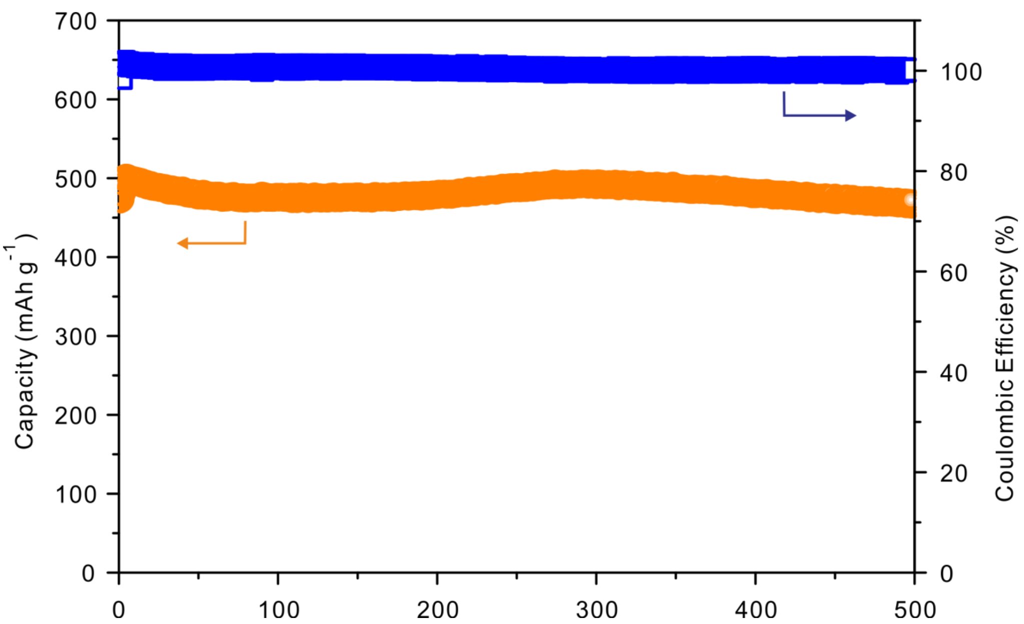


**Figure S7**. Cycling performance of S-$Fe_7S_8$ at a current rate of 4C and the corresponding coulombic efficiency.

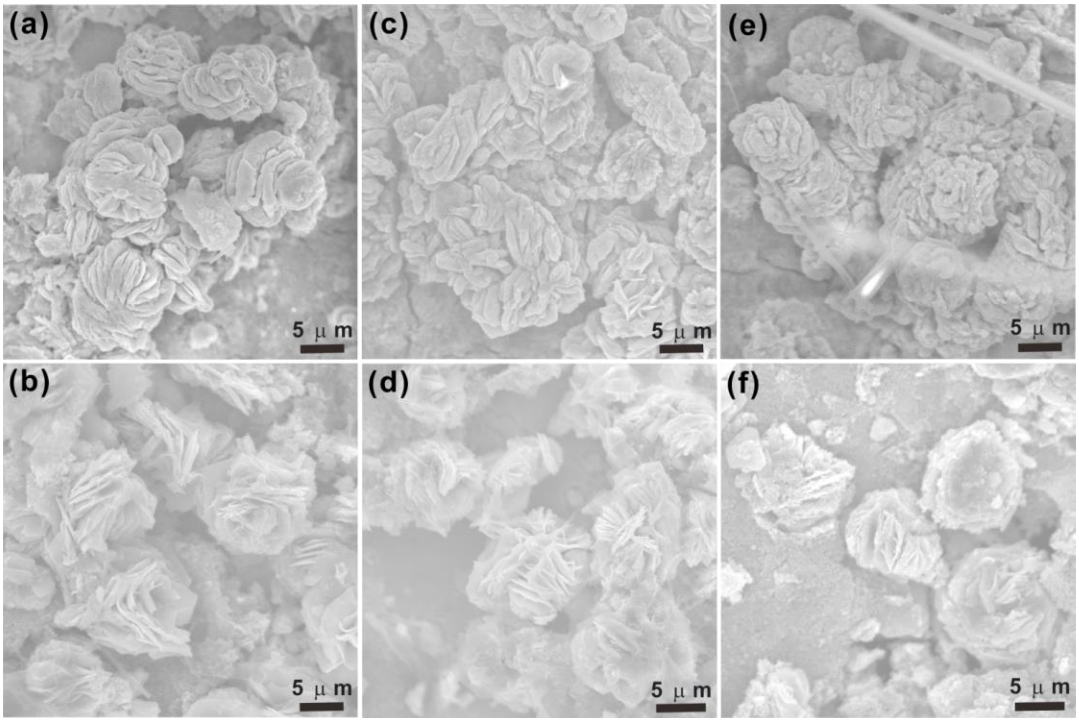


**Figure S8.** FESEM images of S-$Fe_7S_8$ after the 1st discharge (a), the 1st charge (b), the 2nd discharge (c), the 2nd charge (d), the 10th discharge (e), and the 10th charge (f).

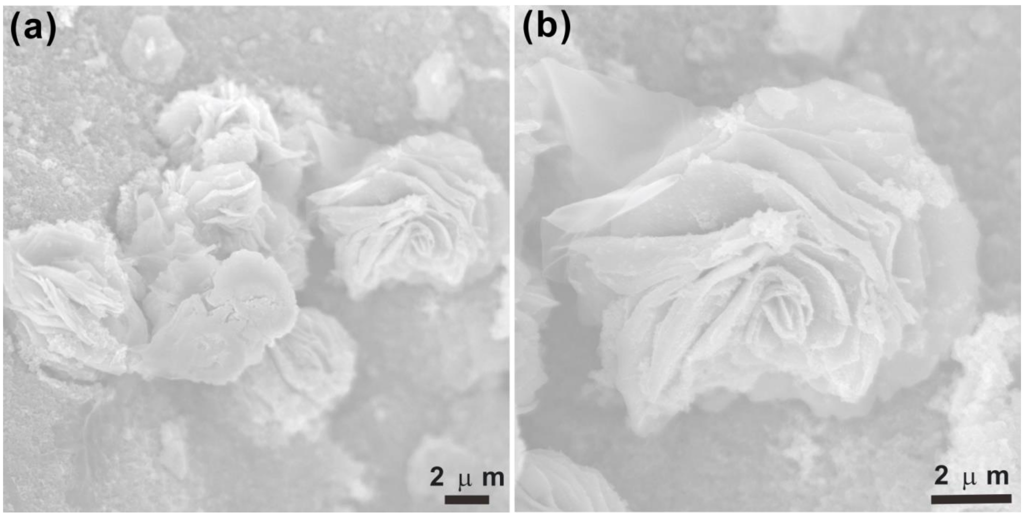


**Figure S9.** FESEM images of S-$Fe_7S_8$ after 100 charge/discharge cycles.

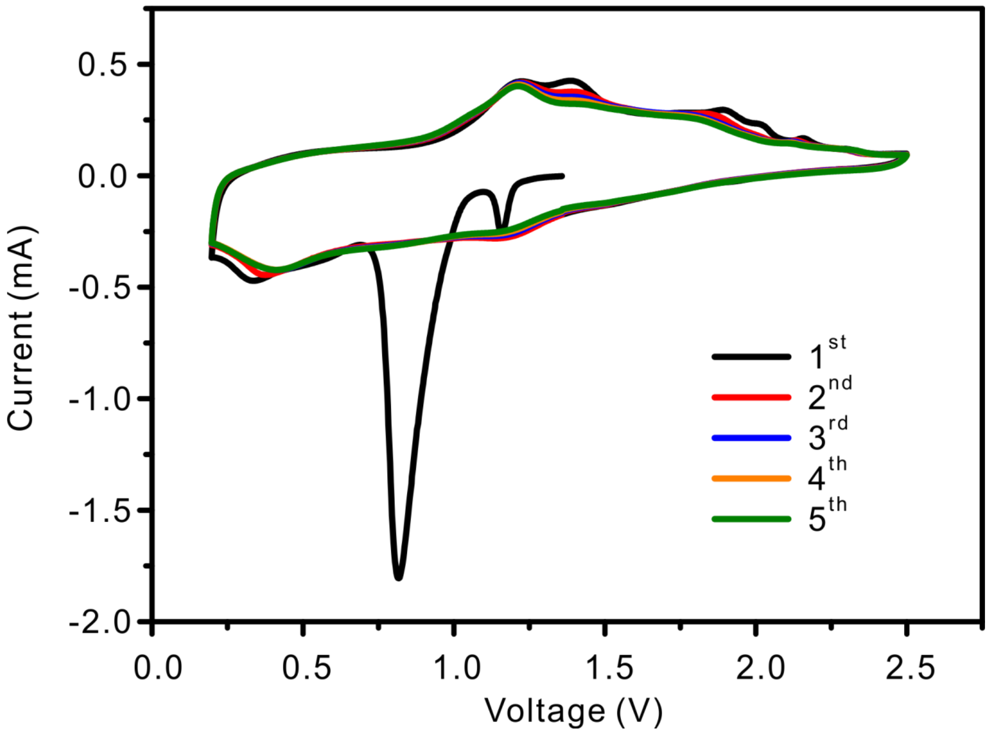


**Figure S10.** CV curves of S-$Fe_7S_8$ for the first five cycles at a scan rate of 0.1 mV $s^{-1}$.

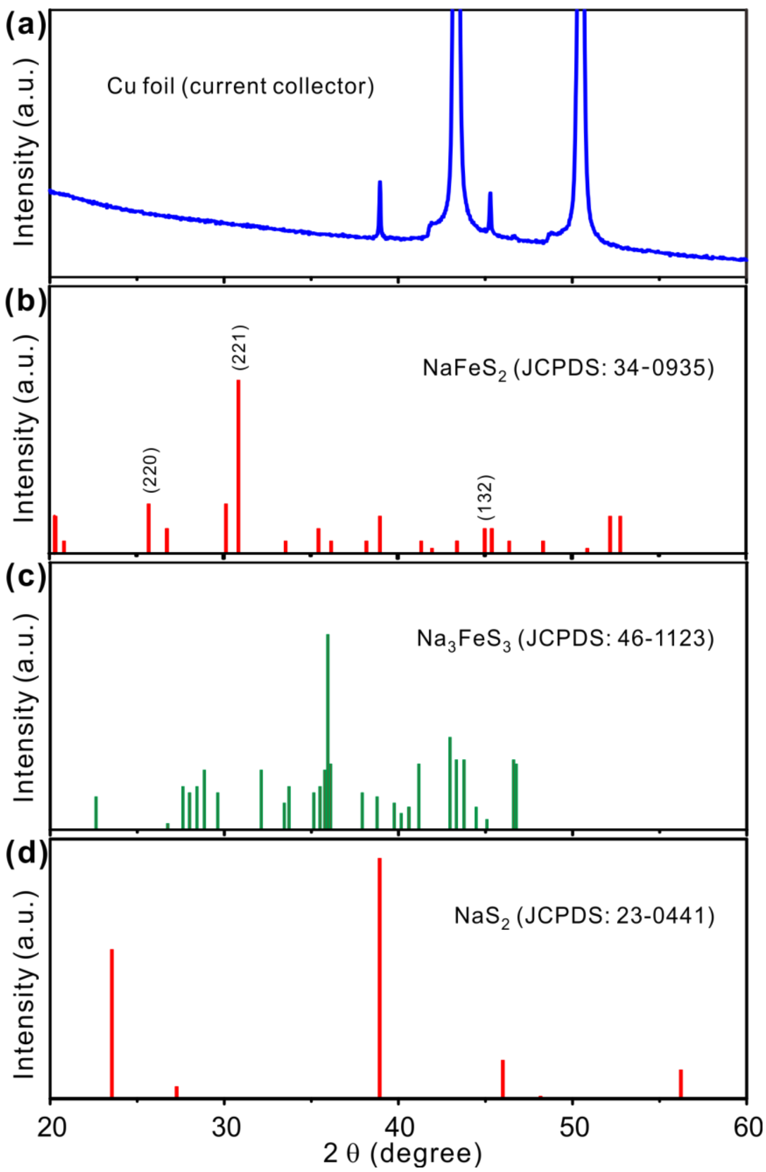


**Figure S11**. XRD pattern of Cu foil (a) and the standard XRD patterns of the different products for sodiation and desodiation (b-d).

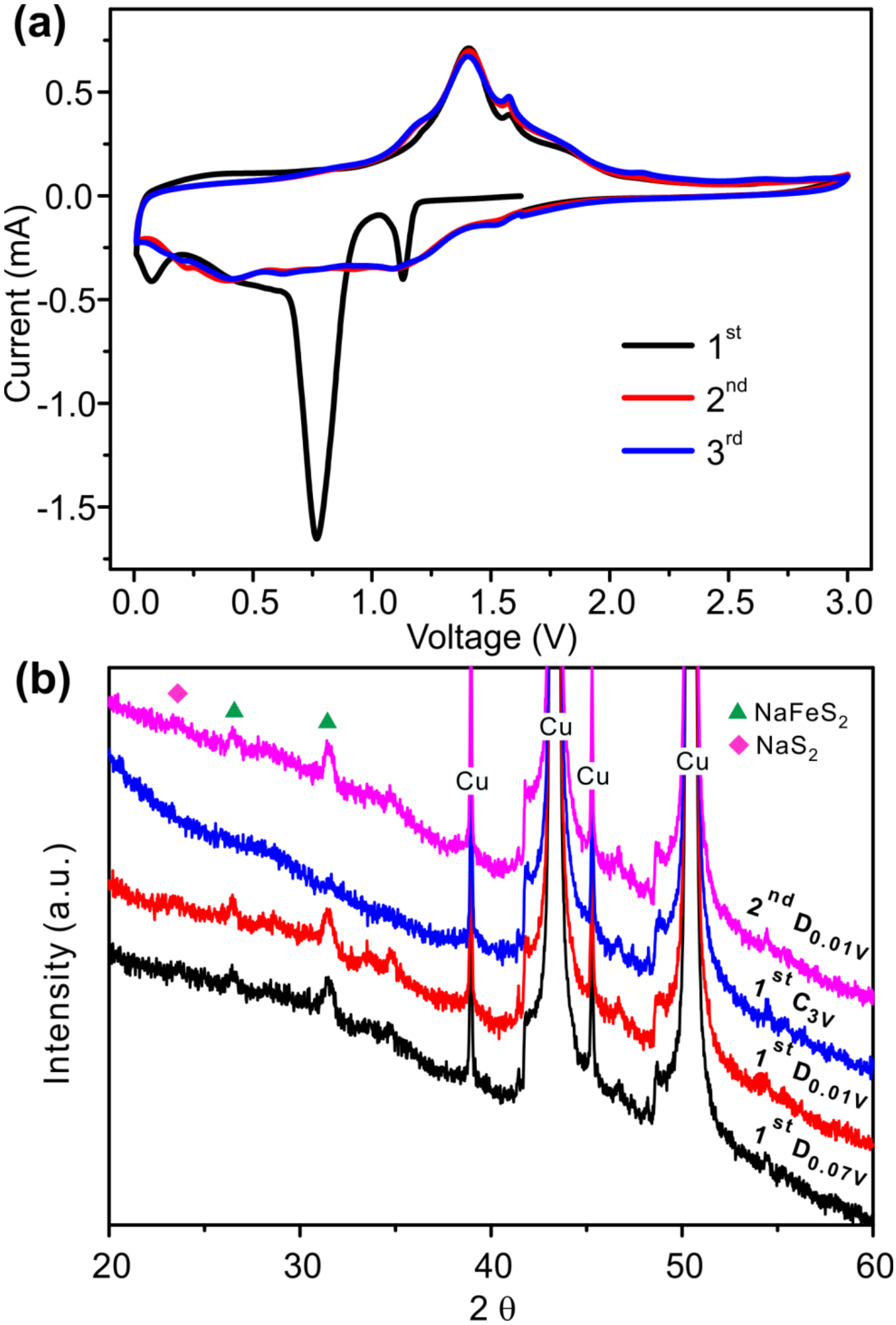


**Figure S12.** (a) CV curves of S-$Fe_7S_8$ for the first five cycles at a scan rate of 0.1 mV $s^{-1}$ between 0.01 and 3 V. (b) Electrochemical mechanism investigation of S-$Fe_7S_8$ during the sodiation/desodiation processes between 0.01 and 3 V: ex-situ XRD patterns of S-$Fe_7S_8$ electrodes in various discharged and charged states for the first and second cycles.

**Table 1.** Comparison of some typical iron sulfides and other metal sulfides anode materials for SIBs.

| Types of materials | [a]Current density [mA $g^{-1}$] | Cycle number | [b]Specific capacity [mAh $g^{-1}$] | References |
|---|---|---|---|---|
| Yolk-shell FeS@C nanospheres | 100 (2500) | 300 | 488 (452) | [1] |
| Graphene coated micron-sized $FeS_2$ | 200 (5000) | 800 | 460 (323) | [2] |
| Greigite $Fe_3S_4$ nanoparticles | 5000 (40000) | 1000 | 401 (233) | [3] |
| $FeS_2$ microspheres anchoring on rGO | 900 (4500) | 800 | 180 (195) | [4] |
| Porous FeS nanofibers | 500 (5000) | 150 | 592 (353) | [5] |
| Co-doped $FeS_2$ nanospheres | 1000 (20000) | 400 | 270 (172) | [6] |
| Pyrite nanocrystals | 1000 (5000) | 600 | 410 (600) | [7] |
| $FeS_2$@C yolk-shell nanobox | 100 (5000) | 100 | 511 (403) | [8] |
| Pyrite $FeS_2$ | 1000 (20000) | 20000 | 180 (170) | [9] |
| $Fe_{1-x}S$/CNT | 500 (8000) | 200 | 449 (326) | [10] |
| FeS-rGO | 500 (6000) | 50 | 547 (340) | [11] |
| FeS@C/carbon cloth | 91 (4600) | 50 | 430 (280) | [12] |
| $Co_9S_8$-C | 500 (1500) | 50 | 404 (326) | [13] |
| $Co_3S_4$@polyaniline | 200 (4000) | 100 | 253 (184) | [14] |
| $CoS_2$-MWCNT | 100 (800) | 100 | 568 (449) | [15] |
| $SnS_2$/NGS | 200 (10000) | 100 | 450 (148) | [16] |
| SnS/C | 1000 (10000) | 300 | 260 (145) | [17] |
| $SnS_2$/Graphene | 200 (4000) | 100 | 619 (326) | [18] |
| CuS-rGO | 100 (4000) | 50 | 393 (345) | [19] |
| S-$Fe_7S_8$ | 200 (10000) | 200 | 515 (390) | Present work |
| | 5000 (20000) | 3500 | 380 (300) | |

Note: the current density values in brackets of column[a] correspond to the capacity values in brackets of column[b].


[1] Y.X. Wang, J. Yang, S.L. Chou, H.K. Liu, W.X. Zhang, D. Zhao, S.X. Dou, Uniform yolk-shell iron sulfide-carbon nanospheres for superior sodium-iron sulfide batteries, Nat. Commun. 6 (2015) 8689.

[2] K. Chen, W. Zhang, L. Xue, W. Chen, X. Xiang, M. Wan, Y. Huang, Mechanism of capacity fade in sodium storage and the strategies of improvement for $FeS_2$ anode, ACS Appl. Mater. Interfaces 9 (2017) 1536-1541.

[3] Q. Li, Q. Wei, W. Zuo, L. Huang, W. Luo, Q. An, V.Q. Pelenovich, L. Mai, Q. Zhang, Greigite $Fe_3S_4$ as a new anode material for high-performance sodium-ion batteries, Chem. Sci. 8 (2017) 160-164.

[4] W. Chen, S. Qi, L. Guan, C. Liu, S. Cui, C. Shen, L. Mi, Pyrite $FeS_2$ microspheres anchoring on reduced graphene oxide aerogel as an enhanced electrode material for sodium-ion batteries, J. Mater. Chem. A 5 (2017) 5332-5341.

[5] J.S. Cho, J.S. Park, Y.C. Kang, Porous FeS nanofibers with numerous nanovoids obtained by kirkendall diffusion effect for use as anode materials for sodium-ion batteries, Nano Res. 10 (2017) 897-907.

[6] K. Zhang, M. Park, L. Zhou, G.H. Lee, J. Shin, Z. Hu, S.L. Chou, J. Chen, Y.M. Kang, Cobalt-doped $FeS_2$ nanospheres with complete solid solubility as a high-performance anode material for sodium-ion batteries, Angew. Chem. Int. Ed. 55 (2016) 12822-12826.

[7] M. Walter, T. Zund, M.V. Kovalenko, Pyrite ($FeS_2$) nanocrystals as inexpensive high-performance lithium-ion cathode and sodium-ion anode materials, Nanoscale 7 (2015) 9158-9163.

[8] Z.M. Liu, T. Lu, T. Song, X.Y. Yu, X.W. Lou, U. Paik, Structure-designed synthesis of $FeS_2$@C yolk–shell nanoboxes as a high-performance anode for sodium-ion batteries, Energy Environ. Sci.10 (2017) 1576-1580.

[9] Z. Hu, Z. Zhu, F. Cheng, K. Zhang, J. Wang, C. Chen, J. Chen, Pyrite $FeS_2$ for high-rate and long-life rechargeable sodium batteries, Energy Environ. Sci. 8 (2015) 1309-1316.

[10] Y. Xiao, J.Y. Hwang, I. Belharouak, Y.K. Sun, Na storage capability investigation of a carbon nanotube-encapsulated $Fe_{1-x}S$ composite, ACS Energy Lett. 2 (2017) 364-372.

[11] S.Y. Lee, Y.C. Kang, Sodium-ion storage properties of FeS-reduced graphene oxide composite powder with a crumpled structure, Chem.-Eur. J. 22 (2016) 2769-2774.

[12] X. Wei, W.H. Li, J.A. Shi, L. Gu, Y. Yu, FeS@C on carbon cloth as flexible electrode for both lithium and sodium storage, ACS Appl. Mater. Interfaces 7 (2015) 27804-27809.

[13] Y.N. Ko, Y.C. Kang, $Co_9S_8$-carbon composite as anode materials with improved Na-storage performance, Carbon 94 (2015) 85-90.

[14] Q. Zhou, L. Liu, Z.F. Huang, L. G. Yi, X.Y. Wang, G.Z. Cao, $Co_3S_4$@polyaniline nanotubes as high-performance anode materials for sodium ion batteries, J. Mater. Chem. A 4 (2016) 5505.

[15] Z. Shadike, M.H. Cao, F. Ding, L. Sang, Z.W. Fu, Improved electrochemical performance of $CoS_2$-MWCNT nanocomposites for sodium-ion batteries, Chem. Commun. 51 (2015) 10486.

[16] Y. Jiang, Y.Z. Feng, B.J. Xi, S.S. Kai, K. Mi, J.K. Feng, J.H. Zhang, S.L. Xiong, Ultrasmall $SnS_2$ nanoparticles anchored on well-distributed nitrogen-doped graphene sheets for Li-ion and Na-ion batteries, J. Mater. Chem. A 4 (2016) 10719-10726.

[17] C.B. Zhu, P. Kopold, W.H. Li, P.A. van Aken, J. Maier, Y. Yu, A general strategy to fabricate carbon-coated 3D porous interconnected metal sulfides: case study of SnS/C nanocomposite for high-performance lithium and sodium ion batteries, Adv. Sci. 2 (2015) 1500200.

[18] Y.C. Liu, H.Y. Kang, L.F. Jiao, C.C. Chen, K.Z. Cao, Y.J. Wang, H.T. Yuan, Exfoliated-$SnS_2$ restacked on graphene as a high-capacity, high-rate, and long-cycle life anode for sodium ion batteries, Nanoscale 7 (2015) 1325-1332.

[19] J. Li, D. Yan, T. Lu, W. Qin, Y. Yao, L. Pan, Significantly improved sodium-ion storage performance of CuS nanosheets anchored into reduced graphene oxide with ether-based electrolyte, ACS Appl. Mater. Interfaces 9 (2017) 2309-2316.